Journal of Alloys and Compounds 508 (2010) 233–237

Contents lists available at ScienceDirect

Journal of Alloys and Compounds

journal homepage: www.elsevier.com/locate/jallcom

Thickness dependence of the $L_{2,3}$ branching ratio of Cr thin films

F. Aksoy[a,b], G. Akgül[a], Y. Ufuktepe[a,*], D. Nordlund[c]

[a] Physics Department, University of Cukurova, 01330 Adana, Turkey
[b] Physics Department, University of Nigde, 51100 Nigde, Turkey
[c] Stanford Synchrotron Radiation Laboratory, 2575 Sand Hill Road, Menlo Park, CA 94025,USA

ARTICLE INFO

Article history:
Received 19 May 2010
Received in revised form 10 July 2010
Accepted 12 July 2010
Available online 17 July 2010

Keywords:
XANES
Cr
Transmission yield
3d Transition metals
Branching ratio
Electron Escape depth

ABSTRACT

We report the electronic structure of chromium (Cr) thin films depending on its thickness using two measures, total electron yield (TEY) and transmission yield mode. The Cr *L* edge X-ray absorption spectroscopy (XAS) spectrum shows strong thickness dependence with broader line widths observed for $L_{2,3}$ edge peaks for thinner films. The white line ratio (L_3/L_2) was found to be 1.25 from the integrated area under each L_3 and L_2 peak and 1.36 from the ratio of the amplitudes of each L_3 and L_2 peak after the deconvolution. Additionally, we show that full-width at half-maximum (FWHM) at the L_2 and L_3 edges and the branching ratio of Cr change as a function of film thickness and these are discussed in detail. Using $L_{2,3}$ resonance intensity variation as a function of film thickness we calculated the electron escape depth and X-ray attenuation length in Cr. Comparing our results with the literature, there was good agreement for the L_3–L_2 ratio although the detailed shape can show additional solid state and atomic effects.

1. Introduction

The X-ray absorption near edge structure (XANES) of 3*d* transition metals at the $L_{2,3}$ absorption edge typically shows intense white lines that correspond to excitations from the 2*p* core state into the 3*d* band [1–5]. For investigating the 3*d* transition metals, $L_{2,3}$ absorption process is a fundamental probe of the empty 3*d* states which involve the excitation of 2*p* electrons into unoccupied *d*-orbital, the overall intensities of *L* edge should depend on the density of the empty *d* states so that the absorption process can be described by the transition $3d^n \rightarrow 2p^5 3d^{n+1}$ [6]. X-ray absorption spectroscopy (XAS) is a suitable fingerprint technique to extract quantitative information from 3*d* metals. The large spin–orbit interaction of the 2*p* core–hole splits the XAS spectrum into two manifolds, which are the L_3 ($2p_{3/2}$) and L_2 ($2p_{1/2}$) levels. Hence, analysis of the $L_{2,3}$ absorption edge could provide information about the electronic and magnetic structure of 3*d* transition metals. This spin–orbit interaction has an important influence on the spectrum, especially on the branching ratio (BR) between L_3 and L_2 peaks. The branching ratio is the fraction of the total transition probability into the $2p_{3/2}$ manifold. The peak intensity ratio should hence give information on the valence band spin–orbit interaction and the electrostatic interaction in the final state [2]. The branching ratio (BR) is defined as the intensity ratio $I(L_3)/[I(L_2)+I(L_3)]$ where $I(L_3)$ and $I(L_2)$ are the measured intensity of the peaks of $j=3/2$ and $j=1/2$ components respectively. However, for a 3*d* transition metal $L_{2,3}$ edge, the relative intensity of these two peaks would be 2–1. This is predicted by one electron band structure calculation but angular momentum coupling affects the branching ratio and it strongly deviates from the 2:1 ideal [7,8], the so-called anomalous branching ratio, which has been the subject of many studies [9,10]. So far various specific mechanisms have been considered to explain the anomalous ratio such as 2*p* spin–orbit coupling, Coulomb and exchange correlation effects of core–hole interaction [11].

Traditionally, XAS measurements are made in transmission mode by measuring the intensity of the X-ray beam before and after the transmission through a thin film, or in total electron yield (TEY) mode by measuring the total number of electrons per incident photon emitted from the sample as a function of photon energy. These two different methods are commonly employed to measure extended fine structure for thin films and bulk samples which both techniques are equivalent [12]. It has been shown that in TEY mode, the total electron emission from the sample is determined by the sample drain current under X-ray illumination. This technique allows probing a layer hundreds of angstroms thick, so that surface cleanliness is less critical. The probing depth of TEY is actually more like 10*s* of Angstrom (as shown in this paper). Hence is considered to be a surface and interface sensitive approach in contrast to Transmission yield measurements. This gives rise to a strong signal at the *L* edge which is proportional to the absorption coefficient [1]. Moreover, the electron escape depth is a characteristic length of the material and can be described as a measure

* Corresponding author.
E-mail address: ufuk@cu.edu.tr (Y. Ufuktepe).

0925-8388/$ – see front matter © 2010 Elsevier B.V. All rights reserved.
doi:10.1016/j.jallcom.2010.07.100

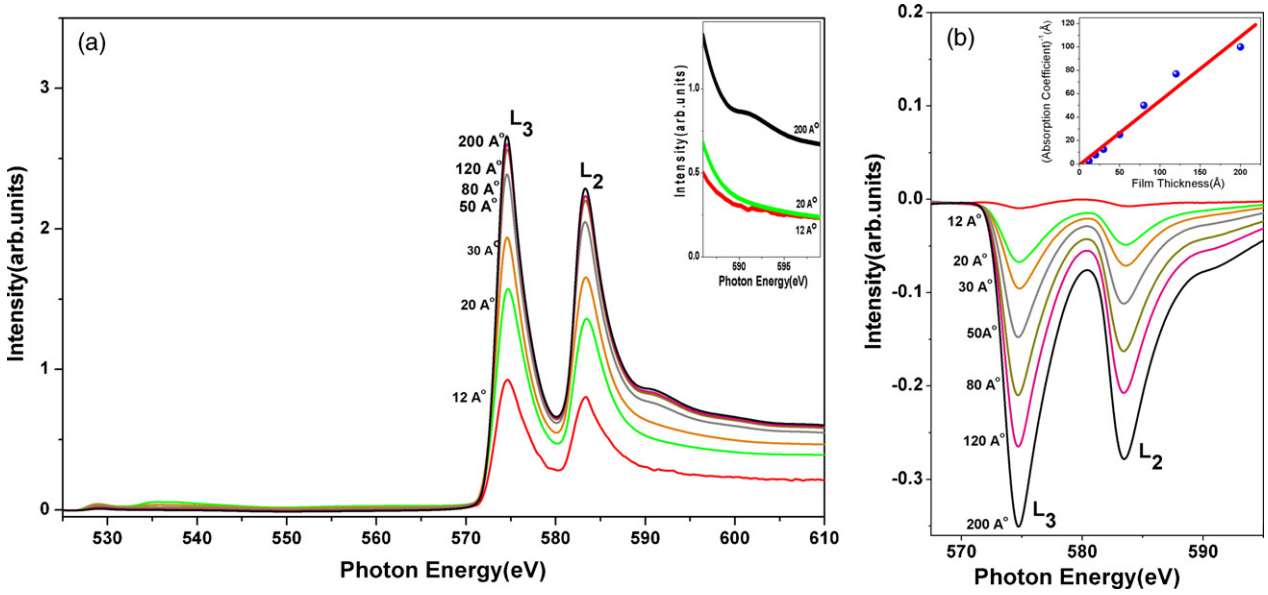

Fig. 1. (a) Normalized total electron-yield (TEY) spectra of Cr films with different film thicknesses. Cr thicknesses in Angstroms (Å) are given beside each curve. The inset of Fig. 1 shows details in the region of 587–595 eV for the 200 Å film together (upper curve) with TEY spectra recorded from 12 and 20 Å films (lower curves). The structure becomes more pronounced for the thicker film compared to thinner Cr films. This structure (hybridization) disappears for the thinner film and becomes visible for increased Cr coverage. (b) Cr $L_{2,3}$ edge absorption spectra recorded in transmission mode. The spectra were normalized and in each spectrum the transmission signal before the onset of the L_3 edge was set to zero just before the peak. The inset shows the plot of the absorption coefficient obtained for the different thicknesses the solid line is a linear curve fit which shows the transmission detection and normalization was linear.

of the depth of elastic and inelastic electrons, that is, photoelectrons, Auger and secondary electrons. Because, the electron escape depth is difficult to calculate, it is unknown for most materials; and it remains uncertain how this length varies from one material to another [13–17].

The purpose of this paper is to contribute to our understanding of the thickness dependence of the Cr $L_{2,3}$ branching ratio intensity and full-width at half-maximum (FWHM) change in this region. We therefore focus on the electronic properties of these films and also extracting the accurate value of electron escaping depth from XAS spectra.

2. Experimental

The experiments were performed at beam line 8.2 of the Stanford Synchrotron Radiation Laboratory (SSRL). Beam line 8.2 is a bending magnet beam line dedicated to probing a wide range of core levels using photoemission, photo-absorption and XANES with an energy range of 100–1300 eV. TEY and transmission spectra were collected at room temperature. Cr films were grown by e-beam evaporation on SiN coated Si wafers. The soft X-ray transparent 100 nm SiN window was centered within a rectangular (4 mm × 1.5 mm) Si wafer that enables performing transmission measurements. For TEY measurements, Cr films were grown on a 200 μm Si wafer, which was the frame of the SiN window. The thickness of the Cr layers, which varied from 12 to 200 Å, was measured with a quartz crystal thin film monitor. The base pressure of the preparation chamber was 1×10^{-10} Torr and below 1×10^{-9} Torr during evaporation. The substrates were mounted on sample holders, which could be transferred without breaking the vacuum between the film growth and measurement chamber. In order to perform transmission measurements, the attenuation of the X-ray flux was assessed by monitoring the incident photon flux with highly transmittive gold grid and measuring the transmitted photon flux with a silicon photodiode mounted just behind the SiN membrane window. The photodiode was operated without a bias voltage and shielded from all light sources except incoming photons passing through the sample. To eliminate the effect of substrates from absorption spectrum, we measured the photo-absorption of the SiN substrate itself just before the Cr deposition. To record the TEY spectra, the sample TEY signal was monitored by the drain current through the wire connecting the otherwise electrically insulated sample to ground, and the number of incoming photons measured by the TEY signal of an 80% transmissive Au net. The ratio of the sample signal and incoming photon flux was then the TEY spectrum of interest for measuring the sample absorption coefficient.

3. Results

Fig. 1(a) shows room temperature XANES spectra for Cr films at the $L_{2,3}$ region with varying thicknesses from 12 to 200 Å in TEY mode. Chromium surfaces are known to be sensitive to oxidation. Data collection was started at 525 eV to permit observing the oxygen 1*s* region to enable verifying the purity of the thin films. Our measurements showed that with the precautions taken, the effect of oxygen on all films could be ignored. We were confident that our thin films were pure metallic Cr films.

Fig. 1(b) represents absorption spectra of Cr thin films at the $L_{2,3}$ region with varying thicknesses in transmission mode. The main features are present in both spectra of Fig. 1(a) and (b) due to the similarity between TEY and transmission measurements [12]. In the transmission spectra, the main peaks were separated by ≈8.8 eV, which showed a typical structure of the Cr *L* edge [18]. The energy separation due to the spin–orbit interaction of Cr 2*p* electrons were observed in the spectra. In each spectrum, the transmission signal before the onset of the L_3 edge at 565 eV was set to zero just before the peak. The main features in the spectrum of Fig. 1 were two maxima at 574.6 and 583.3 eV, which showed a rich multiplet structure above the 2*p* absorption threshold. We observed no detectable energy shift of $L_{2,3}$ edges in the film growing process but the intensity of both peaks were changed as a function of the film thickness. Our high-resolution measurements reveal more structure, which was an additional hump in Fig. 1(a) just after the L_2 edge observed for the films above 50 Å Cr thickness due to transition from 2*p* to 4*s* or 3*d*–4*s* hybrid (mixed) states in the valence band. The inset of Fig. 1(a) shows details of the additional peak in the region of 587–595 eV for the 200 Å thick film (upper curve) together with TEY spectra recorded from 12 and 20 Å films (lower two curves). The structure becomes more pronounced for the thicker film with respect to the thinner one. The first step of the growth regime was most likely to be island formation, which showed the electronic structure of individual Cr islands. It is obvious that the shape of spectra shows strong thickness dependence with broader line widths for thinner Cr films. For consistency, we plotted the absorption coefficient obtained for the different thicknesses, to show the

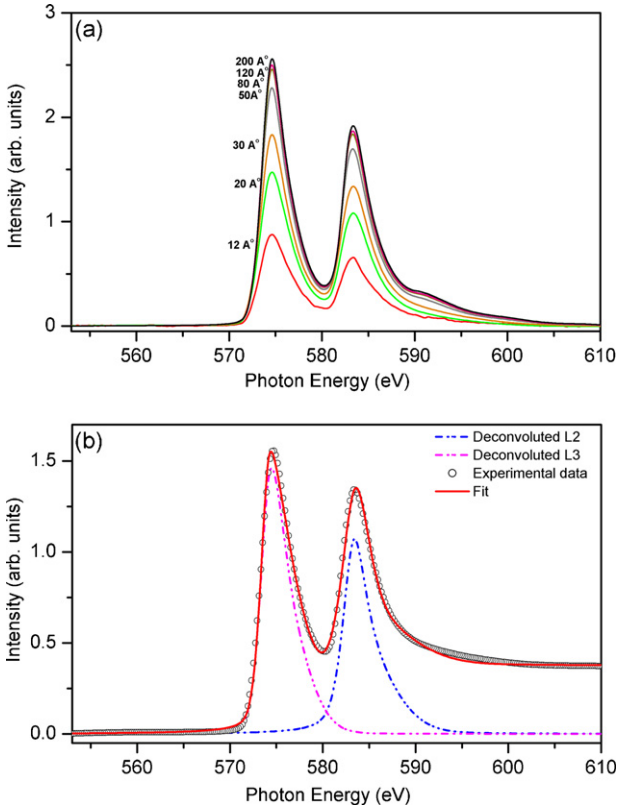

Fig. 2. (a) Normalized and the background-corrected total electron-yield (TEY) spectra of Cr films with different film thicknesses. Cr thicknesses in Angstroms (Å) are given beside each curve. (b) The L_3 and L_2 edges for 20 Å thickness of Cr. Open circles are experimental data. The solid line is the best fit to the experimental data; dashed lines demonstrate deconvoluted Lorentzian functions.

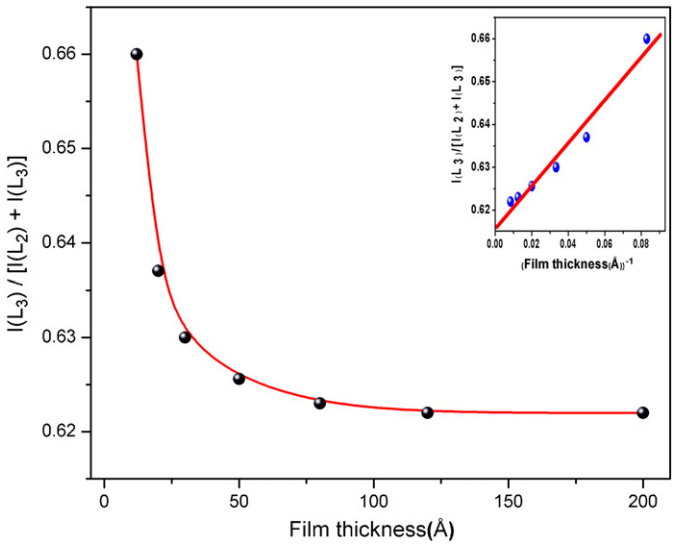

Fig. 3. Branching ratio of the background-corrected intensities at the $L_{2,3}$ edge as a function of Cr film thickness. The drawn line serves only guide the eye. The inset shows the plot of BR intensity versus inverse of the film thicknesses, the solid line is a linear curve fit to experimental data which assumes an ideal layer by layer growth.

transmission detection and normalization was indeed linear (see the inset in Fig. 1(b)).

Thole and Laan pointed out that an electrostatic interaction between *d* electron and valence hole and also spin–orbit correlation of *d* electrons are affecting the BR [2]. To estimate the experimental L_3–L_2 BR intensity $I(L_3)/[I(L_2)+I(L_3)]$ for Cr thin films, we used the normalized L_3 and L_2 peak heights. In general, the L_3 and L_2 XANES spectra include contributions arising from the 2*p*–3*d* transitions as well as excitations from the 2*p* state to continuum states. In order to isolate the excitation spectra only from the inner-shell 2*p* state to the bound 3*d* state, it was necessary to remove the background component. Fig. 2(a) shows both the normalized and the background-corrected TEY spectra of Cr thin films of varying thickness. We consider the intrinsic Lorentzian energy widths due to the finite lifetime of the core–hole. The peaks arising from transitions to bound states in the *d*-band be described by Lorentzians superimposed on the background. In Fig. 2(b), the background-subtracted spectrum for 20 Å Cr thickness was deconvoluted by two Lorentzian functions (corresponding to L_3 and L_2 peaks) separated by spin–orbit splitting. The areas under each function and the amplitudes (intensities) of each function were determined, giving L_3–L_2 ratio of 1.25 for areas and 1.36 for amplitudes. It is crucial to point out here that the best fit (in the Fig. 2b), which is a superposition of two Lorentzian functions, was in good agreement with the experimental data. In measuring the L_3/L_2 ratio from areas by electron energy loss spectroscopy (EELS) Pease et al. [19] report 1.57, Leapman et al. [20] report 1.2 and Ouyang et al. [21] report 1.35. The present TEY result agrees well with the finding of Leapman et al.

Fig. 3 presents the measured branching ratio intensity as a function of the Cr film thickness. The area of the L_3 and L_2 lines would be the correct measure of their intensity, which is proportional to the oscillator strength of the 2*p*–3*d* spin–orbit interaction. It can be seen in Fig. 3 that the BR changed significantly from 0.66 to 0.62 as film thickness increases from 12 to 200 Å. The measured values were consistent with the values obtained from previous research, which were from 0.41 to 0.8 in the 3*d* transition metal series [22]. The inset of Fig. 3 shows the plot of BR versus inverse of the film thicknesses, the solid line is a linear curve fit to experimental data which assumes an ideal layer by layer growth. The growth mode of Cr films shows good agreement with layer by layer model. The plotted curve in Fig. 3 shows that the electronic structure changes little for Cr thin film thicknesses above 80 Å. After this critical thickness, the branching ratio was found to be almost constant and close to bulk value of Cr. The thickness dependency clearly indicates that the spectrum of thin Cr film can be quite different than bulk Cr.

The change in BR intensity is a very large effect due to changing the coordination of the Cr atom from a surface atom to bulk atom with increasing film thickness. The origin of the observed BR decrease with film thickness can be discussed in terms of both 2*p* and 3*d* levels. In the case of 3*d* valence states a broadening of the valence states and increase in *d*-orbital occupation with increasing film thickness are expected. This can be explained by the transition from quasi-atomic to bulk-like structure of thin films resulting in the screening of the 2*p*–3*d* Coulomb interaction due to more delocalized electrons in the thick film. Screening of the core–hole weakens the 2*p*–3*d* Coulomb interaction leading to a small branching ratio. This result reveals that the electron core–hole interaction decreases with film thickness. A similar trend in the $L_{2,3}$ branching ratio in vanadium, cobalt, and chromium clusters has been reported in the literature [23,24].

In order to study the thickness dependence more quantitatively, we examined the full-width at half-maximum at the L_2 and L_3 edges as a function of the Cr film thickness (see Fig. 4). The change of FWHM in Fig 4 cannot be explained by any change of 2*p* core levels, and it can only be related to the change in the unfilled states. The measured L_3 and L_2 FWHM decrease from 4.5 to 3.6 and 4.4 to 3.4 respectively due to change in 3*d* band with Cr thickness. The reduction in FWHM correlated to a reduction in the width of the 3d band. The line width decreases with increasing Cr film thickness resulting in sharp peaks. However the intensity of *L* edge absorption is strongly dependent on 2*p*–3*d* transitions and the number of

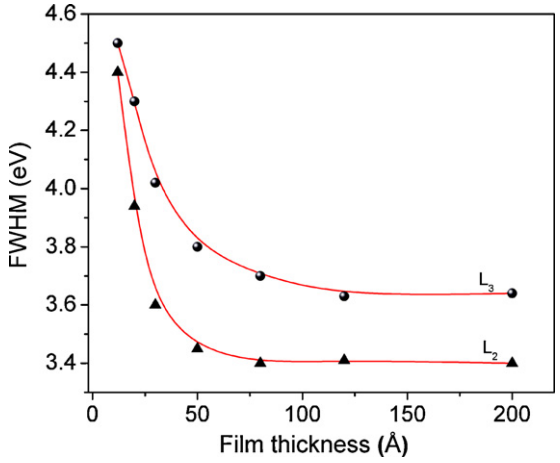

Fig. 4. L_3 and L_2 main peak full-width at half-maximum (FWHM) in the total electron-yield (TEY) as a function of Cr film thickness. The drawn line serves only to guide the eye.

d final states available. When such *d* vacancies are present a strong and sharp peak is observed near the band edge. Therefore the lifetime is very sensitive to the band structure of the unfilled 3*d* band state. Thicker films showed smaller FWHM than thinner films due to the small core–hole lifetime broadening resulting in sharp multiplet structures. It has been shown that the measured white line width for any oxide is less than that of the corresponding metal [25].

The electron escape depth (λ_e) is one of the most important parameters in electron spectroscopy. To calculate (λ_e), we used the model proposed by Thole [26]. In the case of thin films, TEY or transmitted intensity is given by the expression:

$$I(x) \approx I_\infty(1 - e^{-(x/\lambda_e)}) \quad (1)$$

where x is the layer thickness, λ_e is the electron escape depth, and I_∞ is the electron yield from an infinitely thick layer. In Fig. 5 measured values of relative transmitted peak intensities (calculated in Fig. 1b) of $L_{2,3}$ are plotted as a function of film thickness. The solid lines were obtained from best fits of the Eq. (1). We have found from the present data that the best fits correspond to $\lambda_e(L_3) = 25 \pm 2$ Å and $\lambda_e(L_2) = 27 \pm 2$ Å values. Frazer et al. measured the maximum electron escape depth of core level binding energies ranging from

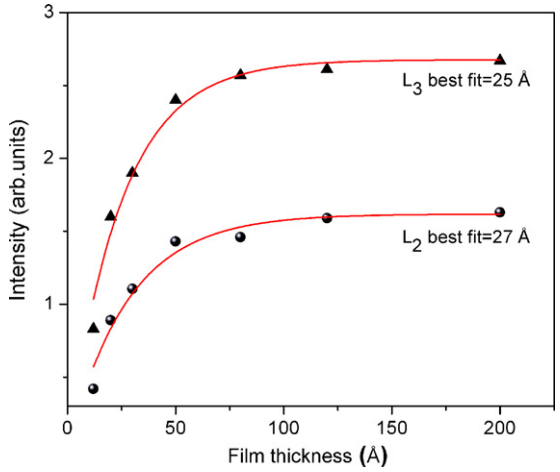

Fig. 5. Normalized peak height of L_3 and L_2 resonance as a function of Cr film thickness. Solid curves result from fitting the function $y = A(1 - e^{-bx})$ to the respective film thickness dependencies. The best-fitting function using the electron escape depth as a free parameter was obtained at 25 and 27 Å for the L_3 and L_2 edges respectively.

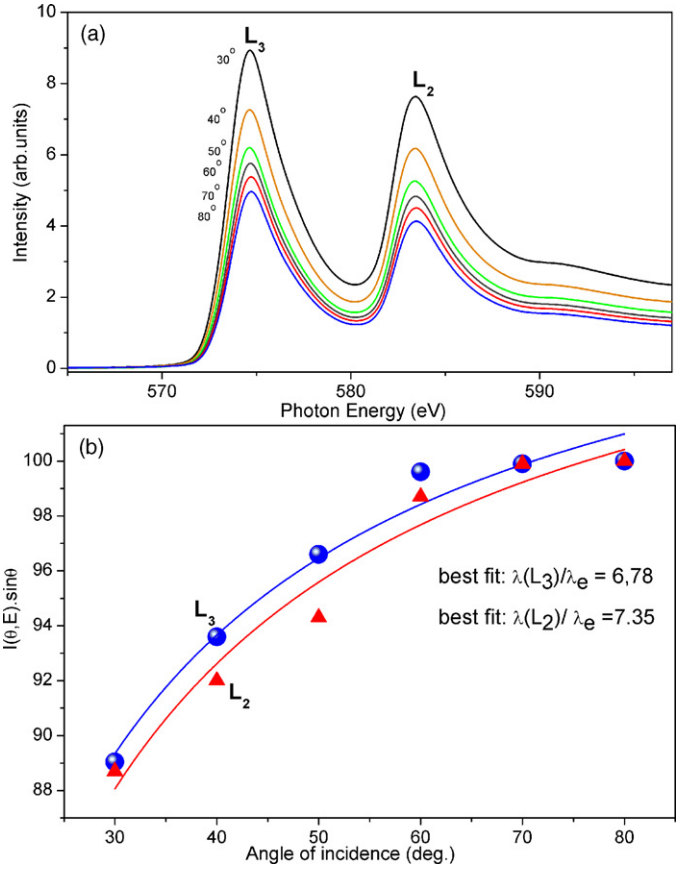

Fig. 6. (a) Normalized Cr *L*-edge XANES spectra for 200 Å film measured at six different incident angles. (b) Angular dependence of Cr $L_{2,3}$ resonance intensity plotted as a function of the angle of incidence of light. Both intensity curves are normalized to 100 for $\theta = 80^\circ$.

77 to 929 eV found to be between 15 and 141 Å [27] but no data is available in the literature for comparison; electron escape depth at $L_{2,3}$ edge is to the best of our knowledge the first to be measured for pure Cr film.

Fig. 6a shows normalized Cr *L* edge TEY-XANES spectra for 200 Å Cr film recorded at six different incident angles with respect to the surface of the sample. The relative intensity is higher in the measured spectra at small X-ray incident angle (30°). When changing from normal to grazing incidence geometry, the TEY signal will increase, since the effective path length within the layer sampled by TEY increases; hence also the number of absorbed photons. For a thick film (x»λ_e) Eq. (1) can be written as

$$I_\theta(\theta, E)\sin\theta \approx \frac{C}{(1/\sin\theta) + (\lambda_x(E)/\lambda_e)} \quad (2)$$

where θ is the angle of incidence of the X-rays, $\lambda_x(E)$ is the X-ray attenuation length at energy *E*. Fig. 6(b) shows the $L_{2,3}$ peak maximum intensities multiplied by $\sin\theta$ and plotted as a function of the X-ray angle of incidence. The solid curves are best fit of Eq. (2) using *C* and $\lambda_x(E)/\lambda_e$ as free parameters. We found that best fits correspond to $\lambda_x(E)/\lambda_e = 6.78$ at the L_3 edge and $\lambda_x(E)/\lambda_e = 7.35$ at the L_2 edge. To obtain X-ray attenuation length we used our calculated electron escape depth values for Cr in Fig. 5. The values obtained for $\lambda_x(E)$ at photon energies corresponding to the maximum of the $L_{2,3}$ edges are $\lambda_x(L_3) \approx 165.9$ Å and $\lambda_x(L_2) \approx 198.45$ Å, respectively.

4. Conclusions

In summary, we performed two experimental series of XAS to obtain L edge branching ratio intensity and electron escape depth of Cr, measured both in TEY and transmission modes. A strong thickness dependence of XAS with Cr film thickness was observed. We used an exponential curve fit of the peak intensities as a function of film thicknesses to derive values of electron escape depth. Furthermore, we found that with decreasing film thickness, the number of d holes decreased and the spin–orbit interaction increased, resulting in higher branching ratio values at the L edge. Thinner film showed atomic-like structure with island growth that turned to a more bulk-like structure as film thickness increased. This demonstrated that FWHM at the $L_{2,3}$ edge changed from 4.5 to 3.4 in pure Cr with increased thickness which showed that the electronic and magnetic structures of Cr thin films differ with respect to bulk. In addition, we present the first results of our systematic investigation of the TEY electron escape depth and X-ray attenuation length of the Cr thin films. The XAS study provides valuable information for investigating surface phenomena and magnetism related electronic states of 3d metals.

Acknowledgments

The authors thank Professor Piero Pianetta, Professor Herman Winick and the staff at the Stanford Synchrotron Radiation Laboratory (SSRL) for their excellent support, where the XANES experiments were carried out. SSRL is supported by the Department of Energy (DOE), Office of Basic Energy Science. Y.U. acknowledges financial support by the University of Cukurova and the DOE Cooperative Research Program for the Synchrotron-light for Experimental Science and Applications in the Middle East (SESAME) project. The authors also thank Fred Johnson for editorial assistance with this manuscript.

References

[1] J. Stöhr, NEXAFS Spectroscopy. Springer Series in Surface Sciences, vol. 25, Springer, Berlin, 1992, chapter 5.
[2] B.T. Thole, G. van der Laan, Phys. Rev. B 38 (1988) 3158.
[3] F. de Groot, A. Kotani, Core Level Spectroscopy of Solids, CRC Taylor & Francis, London, 2008, chapter 6.
[4] H. Wende, Rep. Prog. Phys. 67 (2004) 2105.
[5] A.L. Ankudinov, A.I. Nesvizhskii, J.J. Rehr, Phys. Rev. B 67 (2003) 115120.
[6] G. Van der Laan, B.T. Thole, Phys. Rev. B 43 (1991) 13401.
[7] R.D. Leapman, L.A. Grunes, Phys. Rev. Lett. 45 (1980) 397.
[8] F.M.F. de Groot, Physica B 208 & 209 (1995) 15.
[9] E.Z. Kurmaev, A.L. Ankudinov, J.J. Rehr, L.D. Finkelstein, P.F. Karimov, A. Moewes, J. Electron Spectrosc. Relat. Phenom. 148 (2005) 1.
[10] D.M. Pease, A. Fasihuddin, M. Daniel, J.I. Budnick, Ultramicroscopy 88 (2001) 1.
[11] X. Wang, F.M.F. de Groot, S.P. Cramer, Phys. Rev. B 56 (1997) 4553.
[12] W. Gudat, C. Kunz, Phys. Rev. Lett. 29 (1972) 169.
[13] S. Gota, M. Gautier-Soyer, M. Sacchi, Phys. Rev. B 62 (2000) 4187.
[14] V. Chakarian, Y.U. Idzerda, C.T. Chen, Phys. Rev. B 57 (1998) 5312.
[15] R. Nakajima, J. Stöhr, Y.U. Idzerda, Phys. Rev. B 59 (1999) 6421.
[16] G. Akgül, F. Aksoy, Y. Ufuktepe, J. Luning, Solid State Commun. 149 (2009) 384.
[17] A. Scherz, E.K.U. Gross, H. Appel, C. Sorg, K. Baberschke, H. Wende, K. Burke, Phys. Rev. Lett. 95 (2005) 253006.
[18] U. Arp, K. Iemura, G. Kutluk, T. Nagata, S. Yagi, A. Yagishita, J. Phys. B 28 (1995) 225.
[19] D.M. Pease, S.D. Bader, M.B. Brodsky, J.I. Budinck, T.I. Morrison, N.J. Zaluzec, Phys. Lett. 114A (1986) 491.
[20] R.D. Leapman, L.A. Grunes, P.L. Fejes, Phys. Rev. B 26 (1982) 614.
[21] H. Ouyang, J. Kwan, J. Appl. Phys. 92 (2002) 12.
[22] G. Van der Laan, Physica B 158 (1989) 395.
[23] J.T. Lau, J. Rittmann, V.Z. Bayer, M. Vogel, K. Hirsch, Ph. Klar, F. Lofink, T. Möller, B.V. Issendorff, Phys. Rev. Lett. 101 (2008) 153401.
[24] M. Reif, L. Glaser, M. Martins, W. Wurth, Phys. Rev. B 72 (2005) 155405.
[25] J. Graetz, C.C. Ahn, H. Ouyang, P. Rez, B. Fultz, Phys. Rev. B 69 (2004) 235103.
[26] B.T. Thole, G. van der Laan, J.C. Fuggle, G.A. Sarwatzky, R.C. Karnatak, J.M. Esteva, Phys. Rev. B 32 (1985) 5107.
[27] B.H. Frazer, B. Gilbert, B.R. Sonderegger, G. De Satsio, Surf. Sci. 537 (2003) 161.